Journal of Magnetic Resonance 198 (2009) 105–110

Contents lists available at ScienceDirect

Journal of Magnetic Resonance

journal homepage: www.elsevier.com/locate/jmr

An isotropic chemical shift–chemical shift anisotropic correlation experiment using discrete magic angle turning

Jian Zhi Hu *, Jesse A. Sears, Ja Hun Kwak, David W. Hoyt, Yong Wang, Charles H.F. Peden

Institute for Interfacial Catalysis, Environmental Molecular Sciences Laboratory, Pacific Northwest National Laboratory, 902 Battelle Boulevard, P.O. Box 999, MS K8-98, Richland, WA 99352, USA

ARTICLE INFO

Article history:
Received 10 November 2008
Revised 15 January 2009
Available online 30 January 2009

Keywords:
Isotropic–anisotropic chemical shift correlation
Discrete sample rotation
MAT
MAS
Magnetic susceptibility
High resolution spectrum
In situ detection

ABSTRACT

An isotropic–anisotropic shift 2D correlation spectroscopy is introduced that combines the advantages of both magic angle turning (MAT) and magic angle hopping (MAH) technologies. In this new approach, denoted DMAT for "discrete magic angle turning", the sample rotates clockwise followed by an anticlockwise rotation of exactly the same amount with each rotation less or equal than 360° but greater than 240°, with the rotation speed being constant only for times related to the evolution dimension. This back and forth rotation is repeated and synchronized with a special radio frequency (RF) pulse sequence to produce an isotropic–anisotropic shift 2D correlation spectrum. For any spin-interaction of rank-2 such as chemical shift anisotropy, isotropic magnetic susceptibility interaction, and residual homo-nuclear dipolar interaction in biological fluid samples, the projection along the isotropic dimension is a high resolution spectrum. Since a less than 360° sample rotation is involved, the design potentially allows for *in situ* control over physical parameters such as pressure, flow conditions, feed compositions, and temperature so that true *in situ* NMR investigations can be carried out.

Published by Elsevier Inc.

1. Introduction

Since the pioneering work of Andrew and Eades [1], the magic angle spinning (MAS) experiment has become one of the most useful experiments in the field of NMR. By spinning the sample about an axis inclined at an angle of 54.74° with respect to the external magnetic field and at a sample spinning rate of several kHz or more, a high resolution, high sensitivity isotropic spectrum is produced that is free from line broadening induced by a variety of spin interactions such as chemical shift anisotropy, and magnetic susceptibility and weak homo-nuclear dipolar interactions. The fast-MAS experiment has therefore found widespread application in the study of solid and semi-solid samples, including characterizing organic [2,3] and inorganic solid materials [4,5], biological tissue/cell samples [6–13], and biofluids [14–16], etc.

However, the gain in high spectral resolution and the high sensitivity come with the loss of the anisotropic information that, in general, provides more structural information than the isotropic shift. Furthermore, because of constant fast sample spinning used in MAS, it is very difficult or impossible to carry out a true *in situ* investigation where precise and simultaneous control over pressure, flow, feed composition, and temperature are needed.

To recover the anisotropic information, many two dimensional experiments have been developed during the last three decades [17–37] All of these techniques share the common feature of separating the anisotropic line shape (either as a powder pattern or as a spinning sideband pattern) by isotropic chemical shift differences in the 2D spectral plane. The projection along the isotropic dimension is a high resolution spectrum similar to that obtained from fast-MAS. Among these techniques, the magic angle hopping (MAH) experiment pioneered by Bax et al. [17] has the potential to meet the requirements for *in situ* investigations. In MAH, two successive rapid 120° sample rotations followed by a reverse 240° rotation about the magic angle axis are used. For the times prior to the first 120° rotation, between the two 120° sample rotations and after the second 120° rotation, the magnetization is allowed to precess in the transverse plane. Immediately prior to each 120° rotation, a projection pulse is used to project either the *cosine* or *sine* component of the magnetization to the main field direction.

Since only a total of 240° sample rotation is involved in the MAH experiment, tubes can be connected to the sample chamber, allowing simultaneous control over pressure, feed composition and temperature. Attempts have been made to construct such an MAH probe for *in situ* investigations of catalyst reactions [19]. However, because of the technical difficulties associated with MAH, the method has not found wide applications. For example, it is difficult to maintain the rotation axis precisely at the magic angle. It is equally difficult to achieve precisely the required 120° sample rotations about the magic angle axis, and any errors associated with the rotation angles result in line broadening along the isotro-

* Corresponding author. Fax: +1 509 371 6546.
E-mail address: Jianzhi.Hu@pnl.gov (J.Z. Hu).

1090-7807/$ - see front matter Published by Elsevier Inc.
doi:10.1016/j.jmr.2009.01.027

pic dimension [20]. Consequently, the spectral resolution along the isotropic dimension of MAH is much poorer than that from fast-MAS. Furthermore, the main physical components associated with the hopping probe do not last long because of the significant mechanical wear caused by the rapid hopping–stopping motion used.

In 1992, Gan realized [27] that the effect of each 120° sample rotation in the MAH experiment can be realized by using constant speed sample rotation and then synchronizing the read pulses at 1/3 of rotor periods of sample rotation. Gan's findings have subsequently revolutionized the MAH experiment. A number of improvements [28–34] have been made on Gan's original experiment, with this class of experiments that use slow, constant sample rotation being named magic angle turning (MAT) by Grant's group [30–34]. Compared with the MAH experiment, the MAT experiment is easy to perform for a number of reasons. First, the magic angle can be set experimentally with high accuracy because constant speed sample spinning is used. Second, the read pulses can be spaced accurately at 1/3 of the rotor cycle with the aid of a simple rotor synchronization device [31]. Third, the experiment may be carried out using either simple homemade large-sample-volume probes or commercially available MAS probes [31–34]. Because of the very slow sample spinning employed in the MAT experiment, a large-sample-volume may be used that provides for high sensitivity in the measurements. In addition, it is easy to maintain stable slow sample spinning for long periods of time. As such, MAT probes are very reliable and long-lasting. The MAT experiment, and especially its improved version, i.e., phase-corrected-magic angle-turning (PHORMAT) [31], has been successfully used for measuring principal values of the chemical shift tensor in systems with complex molecular structures [38–40]. Recently the PHORMAT experiment has been extended to obtain high resolution ^{1}H NMR metabolite spectra [41,42], including localized spectra of various organs and tissues in small live animals such as mice [43–46], because ultra-slow sample spinning as low as 1 Hz can be used.

Despite the success with MAT and/or PHORMAT, due to the use of rotation at constant speed the original developments still limit *in situ* investigations where pressure control is required. In this paper, a new method is reported that combines the advantages of both magic angle turning (MAT) and magic angle hopping (MAH) technologies. In the new approach, denoted DMAT for "discrete magic angle turning", the sample rotates clockwise followed by an anticlockwise rotation of exactly the same amount, with each rotation less then or equal to 360° but greater than 240°, and the rotation speed is constant only for times related to the evolution dimension. Since at most 360° sample rotations are involved, gaseous and liquid feed lines may be directly connected to the NMR probe without the plumbing interfering with the mechanics associated with continuous sample rotation. Thus, this design permits *in situ* control over temperature, pressure, flow conditions, and reactant feed composition. The methodology is potentially useful for *in situ* investigations of catalytic reactions under precisely controlled conditions, and for studies that involve biological fluids such as dense cell systems or cells attached to solid surfaces. While further developments in these directions are currently under way, in this paper the basic principles of the DMAT experiment along with the design of a special probe for the NMR measurements will be reported. Preliminary results obtained on solid powder samples of adamantane and 1,2,3-trimethoxybenzene will be used to illustrate principles of the technique.

2. Theory

The DMAT pulse sequence, where the cross-polarization (CP) segment in the original PHORMAT sequence [31] is replaced by a single $\pi/2$ pulse, is given in Fig. 1a. In Fig. 1a, the labels for the timing and phases of the pulses are similar to those in the original report [31] except that the phases of the first pulse, labeled as "a", are changed accordingly to the single pulse version of the experiment (SP-PHORMAT) [41]. The new addition to the SP-PHORMAT is the speed profile of sample rotation depicted in Fig. 1b, which is the key to the DMAT experiment. Briefly, the sample rotor is stationary initially, i.e., $f_0 = 0$ Hz, then the rotation is accelerated with constant acceleration rate "a" (with unit in degree/s^2) during the time period, "t", such that at the end of "t":

$$f_C = a \times t/360, \tag{1}$$

where the unit of f_C is in Hz. This is then followed by a constant speed sample rotation with speed f_C over a period $\geqslant 2T/3 + 2\tau + b_3 + (t_b)_{max}/3 \approx 2T/3 + 2\tau + (t_b)_{max}/3$, where T corresponds to the period of rotation at constant speed f_C, and $(t_b)_{max}$ is the maximal evolution time used in the 2D experiment. At the end of constant rotation period, the rotation is decelerated to $f = 0$ using acceleration with value equal to "$-a$" and over a time period of "t". This is followed by the recycle delay time period of the experiment. Data acquisition (t_a) begins immediately at the end of the last $t_b/3$. The period of t_a can be completely during the constant speed rotation time, or a portion of t_a can be during the constant rotation time with the remainder extending into the deceleration time "t". During the recycle delay time, the rotation is precisely reversed. In practice, the rotation is controlled by a digital encoder. Such a digital encoder has finite resolution "N", e.g., in our system $N = 2000$ counts evenly distributed over a 360° sample rotation. The counts per degree rotation is thus $N/360$. The total number of counts during the acceleration period "t" is thus:

$$\text{Counts} = (a \times t^2/2) \times (N/360). \tag{2}$$

Therefore, by selecting the desired value (an integer) of "Counts" and "f_C", one can find solutions to "a" and "t" based on Eqs. (1) and (2). For example, assuming a constant speed rotation f_C of 2 Hz that needs to be reached during the acceleration time "t" of 110 ms, based on Eq. (1), the acceleration, "a", would be 6545 degrees/s. According to Eq. (2), the number of "Counts" would be about 220, corresponding to 39.6 degrees of sample rotation during "t".

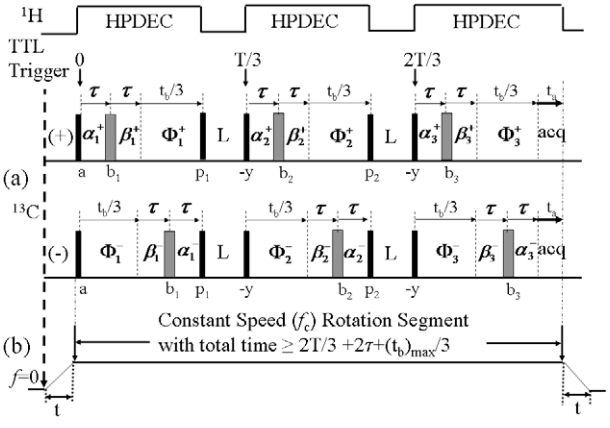

Fig. 1. (a) The SP-PHORMAT pulse sequence, and (b) rotation speed profile used in the discrete magic angle turning (DMAT) experiment. In (a), the $\pi/2$ pulses are represented by black narrow rectangles; the π pulses are shaded grey. Projection pulses are labeled by "p_1" and "p_2" while read out pulses are synchronized at "0", "$T/3$" and "$2T/3$", where T denotes the period of rotation corresponding to the constant speed rotation segment in (b). The magnetization precesses in the transverse plane during the periods labeled α_1, β_1, Φ_1, α_2, β_2, Φ_2, α_3, β_3, and Φ_3, and is along the longitudinal axis during the periods labeled "L"; τ is an echo delay time determined by the probe ringdown and receiver recovery time, and "t" is the time for acceleration or deceleration.

A detailed theory for the PHORMAT experiment has been reported previously [31], and the DMAT is a straightforward extension of this PHORMAT theory. In Fig. 1a, the magnetization precesses in the transverse plane during the periods labeled by the total phase accumulation angles, α_1, β_1, Φ_1, α_2, β_2, Φ_2, α_3, β_3, and Φ_3, and is along the longitudinal axis during the periods labeled "L"; τ is an echo delay time determined by the probe ringdown and receiver recovery time. Keeping in mind that the function of each π pulse is to negate the phase of the magnetization, the projection pulses labeled by p_1 and p_2 project either the cosine or the sine component of the magnetization to the external magnetic field direction. During L, the component of magnetization that remains in the transverse plane is destroyed by either dipolar dephasing (in the case of solids), or by pulsed field gradients (for the case of biological samples). It follows from Refs. [31] and [41] that, for the (+) sequence, by selecting the phases of the pulses and adding 32 individual FIDs together [41], the following combined FID is obtained:

$$F^+ = e^{i((\beta_1^+ + \beta_2^+ + \beta_3^+) - (\alpha_1^+ + \alpha_2^+ + \alpha_3^+) + (\Phi_1^+ + \Phi_2^+ + \Phi_3^+))} F_a(t_a) \quad (3)$$

Where $F_a(t_a)$ corresponds to the FID along the acquisition dimension t_a, which is a powder average of the response in a solid powder sample. It follows from Ref. [31] that

$$\alpha_1^+ + \alpha_2^+ + \alpha_3^+ = \int_0^\tau [\omega(\gamma(t)) + \omega(\gamma(t+T/3)) + \omega(\gamma(t+2T/3))]dt \quad (4)$$

$$\beta_1^+ + \beta_2^+ + \beta_3^+ = \int_0^\tau [\omega(\gamma(t+\tau) + \omega(\gamma(t+\tau+T/3)) + \omega(\gamma(t+\tau+2T/3))]dt \quad (5)$$

$$\Phi_1^+ + \Phi_2^+ + \Phi_3^+ = \int_0^{t_b/3} [\omega(\gamma(t+2\tau)) + \omega(\gamma(t+2\tau+T/3)) + \omega(\gamma(t+2\tau+2T/3))]dt \quad (6)$$

Since T is the rotor period during the constant speed rotation period, the angles $\gamma(x)$, $\gamma(x+T/3)$ and $\gamma(x+2T/3)$, where $x = t$, $t+\tau$, and $t+2\tau$, respectively, describe rotor positions equally spaced at 120° around the axis of rotation. When the rotation axis is inclined at the magic angle with respect to the external field, these three rotor positions put the static magnetic field in three mutually perpendicular directions when viewed from the sample. For a spin subject to a second-rank interaction such as the chemical shift anisotropy, magnetic susceptibility interaction, and weak dipolar coupling, the resonant frequencies at these mutually perpendicular field direction average to the isotropic value of the interaction. Thus,

$$\omega(\gamma(x)) + \omega(\gamma(x+T/3)) + \omega(\gamma(x+2T/3) = 3\omega_{iso} \quad (7)$$

where ω_{iso} is the resonant angular frequency of the isotropic shift. Hence, Eq. (3) becomes:

$$F^+ = e^{i\omega_{iso}t_b} F_a(t_a) \quad (8)$$

Similarly, for the (−) pulse sequence in Fig. 1a, it is obtained that:

$$F^- = e^{-i\omega_{iso}t_b} F_a(t_a) \quad (9)$$

The cosine and the sine components of the FID along the evolution dimension are obtained by adding and subtracting the F^- and F^+ according to Ref. [31] to obtain the Hyper-complex 2D FID. Then a 2D Fourier transformation generates a pure adsorption 2D spectrum where the projection along the isotropic dimension is a high resolution isotropic spectrum, while the projection along the acquisition dimension is an anisotropic pattern.

Note that the derivations for Eqs. (4)–(9) only require a constant speed rotation during the evolution time of the experiment; i.e., during a time starting from "0" to $2T/3 + 2\tau + t_b/3$ in Fig. 1a. By forcing a constant rotation time $\geqslant 2T/3 + 2\tau + (t_b)_{max}/3$, where $(t_b)_{max}$ is the maximal evolution time used in the 2D experiment, an isotropic–anisotropic 2D spectrum is obtained. This gives the discrete magic angle turning (DMAT) approach, where the speed profile of sample rotation is given in Fig. 1b.

3. The DMAT apparatus

The DMAT apparatus is shown in Fig. 2A. It consists of three units, including (a) an NMR probe that is capable of discrete sample rotation about the magic angle axis, (b) a DC Servo motor whose rotation is precisely controlled by (c) a computer programmed control box. The Servo motor is firmly mounted onto a thick aluminum base. The rotation speed profile of the Servo motor, defined in Fig. 1b, is transferred to the NMR probe via a set of teethed belts and pulleys such that the rotation speed profile of the sample rotor is the same as that of the Servo motor.

3.1. The NMR probe

A close-up picture of the prototype DMAT probe is highlighted in Fig. 2B, and key parts of the probe are described next. (i) A mechanism for changing the direction of sample rotation from a rotation about the magic angle axis to a rotation about an axis that is perpendicular to the main magnetic field direction. This is achieved using the teethed pulleys and belts as illustrated in Fig. 2B "1–5". To facilitate the explanation, a drawing containing only the pulling assembly is highlighted in Fig. 2C. One end of a teethed pulley assembly, "1", made of Vespel material, fits tightly around a commercial zirconium rotor with dimensions of 7.5 mm OD and 6 mm ID. To achieve the required tight fit, the pulley assembly is precooled in liquid nitrogen for a few minutes immediately prior to insertion of the rotor. The sample is then loaded at RT, followed by inserting a plug to the other end of the sample rotor. A flat belt, "2", with one face having teeth that match those of the pulley ("1") is used to drive the rotation of the sample. The alignment angle of the belt is changed via two pulleys, "3", with flat surfaces that are rotating in opposite directions so that the other end of this teethed belt fits into a second pulley, "4", that is identical to the one at-

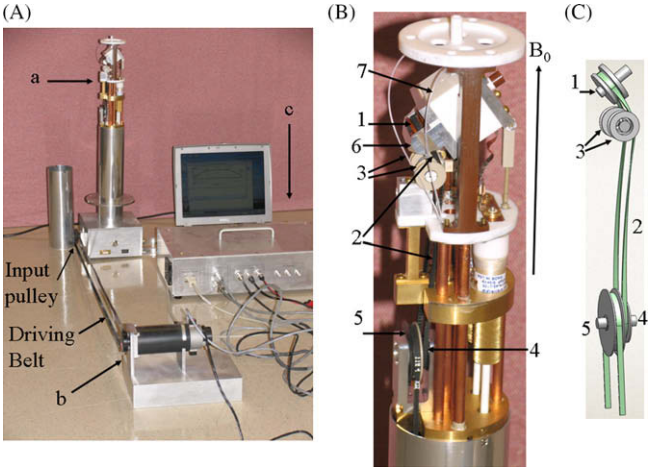

Fig. 2. (A) Picture of the DMAT apparatus showing: (a) the NMR probe; (b) the DC Servo motor; and (c) the computer programmable control box. (B) Close-up picture of the NMR probe with various parts labeled: (1) the teethed pulley assembly (i.e., the DMAT sample rotation module) that fits into the sample rotor; (2) the first teethed driving belt; (3) the two pulleys with flat surfaces that are rotating in opposing directions, which are used to change the directions of rotation of the belt (2); (4) a teethed pulley that is identical to (1); and (5) a teethed pulley that is integrated with (4) such that a full rotation of (5) causes a full rotation of (4), (5) is then connected to the input pulley of the NMR probe as shown in (A). (C) The drawing containing only the pulling assembly in (B) for changing the direction of sample rotation from a rotation about the magic angle axis to a rotation about an axis that is perpendicular to the main magnetic field direction.

tached to the sample rotor (i.e., "1") but its rotor axis is perpendicular to the main magnetic field direction, B_0. In this way, the rotation of the sample rotor about the magic angle axis is changed to the rotation of a pulley, "4", with its axis perpendicular to B_0, which is extended to the input pulley of the probe via another teethed pulley, "5", whose rotation is synchronized with pulley "4". In practice, pulleys "4" and "5" are integrated together so that they rotate at the same speed. (ii) A mechanism for precisely turning the magic angle. A quick-release module, "6", allows the sample/pulley assembly "1" to be easily removed. A fast spinning module (not shown) with a typical pencil type MAS probe design can be quickly mounted to the lower end of the stator, "7", such that the system operates as a typical fast-MAS probe. The fast MAS module is for setting up the magic angle using, e.g., KBr. (iii) An air bearing for the sample rotor is used. The advantages of using an air bearing are that the rotation axis of the sample can be precisely maintained. The device also lasts longer due to the protection of the air bearing from wearing out the supports.

3.2. The DC Servo motor

A commercial DC Servo motor, with an encoder having a 2000 element resolution for a full rotation was purchased from Cleveland Motion Control (PM SERVO MOTOR MOD ME2130-1988, Billerica, MA, USA).

3.3. The computer programmable control box

The computer programmable speed controller (Model DMC-1414) was purchased from Galil Motion Control, Inc., Rocklin CA, USA. The DMC-141 is an encased stand-alone, self-contained device that provides multiple and various interfaces, including, e.g., computer interconnects for speed programming, connections for receiving a TTL trigger signal from the NMR spectrometer, etc. A home-made Visual Basic program was used to realize the speed profile given in Fig. 1b. The motion is initiated by a trigger TTL signal sent out from the pulse sequence given in Fig. 1a.

A driving belt of desired length (~1 m) links the pulley of the DC Servo motor and the input pulley of the NMR probe as indicated in Fig. 2A. The length of the belt is determined by the stray magnetic field since the DC Servo motor contains a small amount of iron that makes the motor paramagnetic. In the current configuration, a belt length of about 1 m is sufficient to place the motor in a location that is safe for operation. The pulley of the Servo motor and the input pulley of the probe, as well as the pulley labeled as "5" in Fig. 2B are identical. Since "5" and "4" in Fig. 2B rotate at the same speed and pulley "4" is identical to that of pulley "1" in Fig. 2B, the rotation speed profile of the sample rotor is the same as that of the DC Servo motor.

4. Experimental results and discussion

All experiments were performed on a Varian-Chemagnetics 300 MHz Infinity spectrometer, operating at Larmor frequencies of 75.438 and 299.9835 MHz for ^{13}C and ^{1}H, respectively. The magic angle was set using KBr with the high speed spinning module of the probe mounted. Fig. 3 shows a ^{13}C CP/MAS spectrum of 1,2,3-trimethoxybenzene that was obtained at a sample spinning rate of 3.05 kHz after setting the magic angle. The peaks corresponding to the C_1 and C_3, differing by 0.46 ppm, are partially resolved. This spectral resolution is identical to what can be obtained with a regular commercial fast-MAS probe at the same magnetic field. This result indicates that the magic angle is set with accuracy similar to commercial probes.

The quick-release mechanism of the probe, labeled as "6" in Fig. 2B, allows for the high spinning module to be replaced by the DMAT module without affecting the rotation angle of the sample rotor. In this way the magic angle is maintained in the DMAT experiment. Fig. 4 shows the 2D ^{13}C DMAT spectrum of adamantane obtained using the SP-DMAT pulse sequence in Fig. 1. Fig. 4a shows the isotropic–anisotropic 2D correlation spectrum, where F_2 and F_1 correspond to the chemical shift anisotropic and isotropic shift dimensions, respectively. The anisotropic projection, given in Fig. 4b, is obtained by summing all of the data on to the F_2 axis. The corresponding half line width, defined as line width at the half height peak positions, is about 177 Hz. In this case, the chemical shift anisotropy is small. Fig. 4c gives the isotropic projection, where the half line width is approximately 30 Hz, approaching that (e.g., about 10 Hz) usually obtainable with a high performance commercial fast-MAS probe.

By replacing the first pulse labeled as "*a*" in Fig. 1 with a CP segment, a CP version of the DMAT experiment, i.e., CP-DMAT, can be generated in the same way as previously reported in the PHORMAT experiment [31]. The results of such an experiment obtained on 1,2,3-trimethoxybenzene (1,2,3-TMB) are summarized in Fig. 5. Compared with the results previously obtained using magic angle hopping (MAH) on 1,2,3-TMB [20], the spectral resolution along the isotropic dimension (Fig. 5c) is significantly enhanced owing to the more accurate angle setting in this one step rotation of the DMAT experiment. In fact, spectral resolution along the isotropic dimension of DMAT is similar to that obtained using a regular MAT experiment with constant speed rotation and similar ^{1}H decoupling strength [33]. For example, in both the DMAT (Fig. 5c) and the MAT [33] experiments, the peaks corresponding to methoxy carbons M_2 and $M_{1,3}$ are well resolved. It may even be possible to resolve M_1 and M_3, as shown for the case of a fast MAS spectrum given in Fig. 3, if an increased decoupling strength is used, which is limited in the current experiments to only about 38 kHz with the presently available probe. Fig. 6 shows the anisotropic powder patterns corresponding to $C_{1,3}$ and C_2 in 1,2,3-TMB, from which it can be determined that the difference between the principal values of δ_{11} and δ_{33} are 145 and 108 ppm for $C_{1,3}$ and C_2, respectively. The isotropic line widths obtained from Fig. 5c are about 2 ppm, where a line narrowing factor of 54–72 was achieved. These results unambiguously prove that the DMAT experiment works equally as well as the previously reported traditional MAT using constant speed rotation.

5. Conclusions

For proving the concept of a new so-called DMAT method, we have demonstrated that a chemical shift anisotropic–isotropic 2D

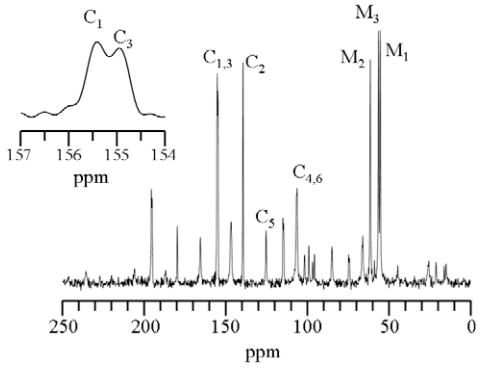

Fig. 3. ^{13}C CP/MAS spectrum of 1,2,3-trimethoxybenzene obtained at a sample spinning rate of 3.05 kHz and using the high speed spinning module of the DMAT probe. The peaks that are unlabeled are spinning sidebands from the various labeled isotropic peaks. The figure inset shows expanded peaks corresponding to the C_1 and C_3 carbons of 1,2,3-TMB that differ by 0.46 ppm. This spectrum was obtained using a contact time (CP) of 2 ms, and by adding eight scans with a recycle delay time of 5 s. The $\pi/2$ pulse width for the initial ^{1}H was 6.5 μs, and the ^{1}H field strengths were about 38.5 and 30 kHz during CP and decoupling periods, respectively.

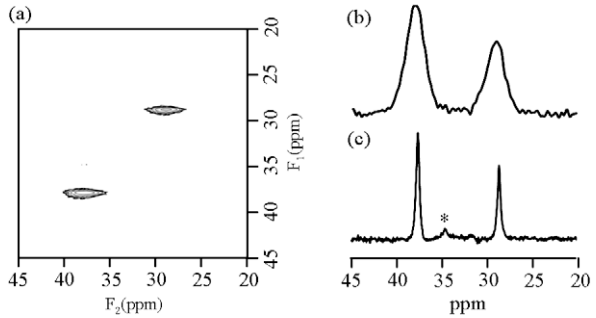

Fig. 4. ^{13}C NMR spectra of adamantane obtained by SP-DMAT: (a) the isotropic–anisotropic 2D correlation spectrum; (b) the anisotropic projection that was obtained by summing all of the data onto the acquisition dimension, i.e., the F_2 axis; and (c) the isotropic projection that was obtained by summing all of the data onto the evolution dimension, i.e., the F_1 axis. The peak labeled by "*" is a probe background signal. The 2D data were acquired using the following parameters. The rotation speed corresponding to the constant speed rotation segment was 2 Hz, i.e., T = 500 ms. The acceleration time, denoted by "t" in Fig. 1, from 0 to 2 Hz was about 110 ms. The first pulse labeled by "a" was triggered 4 ms after the constant speed was reached, and the recycle delay time was 3 s. The free-induction decays in the acquisition dimension (t_2) contained 256 complex points and were transformed to spectra with a spectral width of 10 kHz. The 2D data were collected using 200 t_1 steps, incremented by 500 μs, corresponding to a maximum evolution time of 100 ms and an evolution spectral width of 2 kHz. 2D data sets were acquired with the (+) and the (−) SP-DMAT pulse sequences in Fig. 1 using a total of 64 scans at each t_1 value, resulting in a total measuring time of about 11 h. Hyper-complex 2D data sets were constructed according to the procedure detailed in Ref. [31] using a macro driven program developed on the Varian-Chemagnetics Infinity Spectrometer.

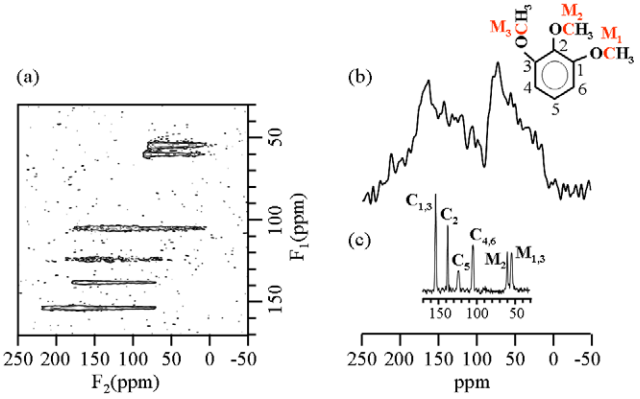

Fig. 5. (a) 2D contour plot of a ^{13}C CP-DMAT spectrum of 1,2,3-trimethoxybenzene (1,2,3-TMB). (b) Anisotropic power pattern that was obtained by summing all of the data onto the F_2 axis. (c) High resolution isotropic projection that was obtained by summing of all the data onto the F_1 axis. The 2D data were acquired using following parameters. The rotation speed corresponding to the constant speed rotation segment was 3.5 Hz, i.e., T = 285.7 ms. The acceleration time, denoted by "t" in Fig. 1, from 0 to 3.5 Hz was about 68 ms. The first pulse labeled by "a" was triggered 4 ms after the 2 Hz speed was reached, and the recycle delay time was 5 s. The free-induction decays in the acquisition dimension (t_2) contained 128 complex points and were transformed to spectra with a spectral width of 40 kHz. The 2D data were collected using 70 t_1 steps, incremented by 90 μs, corresponding to a maximum evolution time of 6.3 ms and an evolution spectral width of 11.11 kHz. 2D data sets were acquired with the (+) and (−) DMAT pulse sequences in Fig. 1 using a total of 256 scans at each t_1 value, resulting in a total measuring time of about 25 h. The ^1H B_1 field during both CP and decoupling periods was about 38 kHz.

correlation spectrum can be obtained for solid powder samples of adamantane and 1,2,3-trimethoxybenzene using only one rotation greater than 240° but less than 360°, that is followed by exactly the same amount of a reversed rotation. In principle, for any spin-interaction of rank-2 such as chemical shift anisotropy, isotropic magnetic susceptibility interaction, and residual homo-nuclear dipolar interaction in biological fluid samples, the projection along

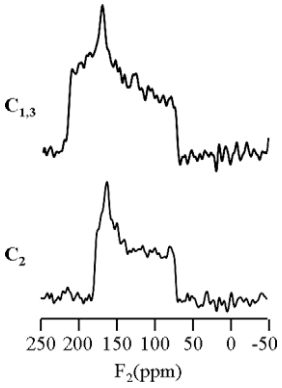

Fig. 6. The sliced chemical shift powder patterns corresponding to $C_{1,3}$ and C_2 carbons of 1,2,3-TMB obtained from the 2D DMAT spectrum in Fig. 5a. These spectra were obtained by selecting a slice at the center of the isotropic chemical shift position of the peak and in parallel to the F_2 axis.

the isotropic dimension is a high resolution spectrum. Importantly, the DMAT method has the potential to permit simultaneous *in situ* control over pressure, temperature, flow conditions, and feed composition, and should, therefore, find many useful applications for *in situ* investigations of catalytic reactions, complementing the elegant constant fast-MAS *in situ* technologies developed by Hunger et al. [47,48]. In addition, biological systems such as dense cell systems or cells attached to solid surfaces, where tubes need be attached to a sealed sample rotor for controlling the physiological conditions, can also be readily investigated.

Acknowledgments

This work was supported by the US Department of Energy (DOE), Office of Basic Energy Sciences, Division of Chemical Sciences, and by a Capability Development Project funded by the Environmental Molecular Science Laboratory, a national scientific user facility sponsored by the DOE Office of Biological and Environmental Research, and located at the Pacific Northwest National Laboratory. PNNL is operated for DOE by Battelle Memorial Institute under Contract No. DE-AC06-76RLO-1830. The authors gratefully acknowledge Mr. Eric Y. Choi for his assistance in building the DMAT controller interface and driving software, Mr. R. James Ewin for his assistance in designing the DMAT probe, and the EMSL machine shop for constructing the DMAT probe.

References

[1] E.R. Andrew, R.G. Eades, Removal of dipolar broadening of NMR spectra of solids by specimen rotation, Nature 183 (1959) 1802.
[2] M.J. Duer (Ed.), Solid-State NMR Spectroscopy: Principles and Applications, Blackwell Publishing, 2002.
[3] K. Schmidt-Rohr, H.W. Spiess, Multidimensional Solid-State NMR and Polymers, Academic Press, 1994.
[4] K.J.D. Mackenzie, M.E. Smith, Multinuclear Solid-State NMR of Inorganic Materials, Pergmon, New York, 2002.
[5] A.T. Bell, A. Pines, NMR Techniques in Catalysis, Marcel Dekker, Inc., 1994.
[6] L.L. Cheng, M.J. Ma, L. Becerra, T. Ptak, I. Tracey, A. Lackner, R.G. Gonzalez, Quantitative neuropathology by high resolution magic angle spinning proton magnetic resonance spectroscopy, Proc. Natl. Acad. Sci. USA 94 (1997) 6408–6413.
[7] M.E. Bollard, S. Garrod, E. Holmes, J.C. Lindon, E. Humpfer, M. Spraul, J.K. Nicholson, High-resolution ^1H and ^1H–^{13}C magic angle spinning NMR spectroscopy of rat liver, Magn. Reson. Med 44 (2000) 2901–2907.
[8] J. Chen, B.M. Enloe, C.D. Fletcher, D.G. Cory, S. Singer, Biochemical analysis using high-resolution magic angle spinning NMR spectroscopy distinguishes lipoma-like well-differentiated liposarcoma from normal fat, J. Am. Chem. Soc. 123 (2001) 9200–9201.
[9] S. Garrod, E. Humpfer, M. Spraul, S.C. Connor, S. Polley, J. Connelly, J.C. Lindon, J.K. Nicholson, E. Homes, High-resolution magic angle spinning ^1H NMR spectroscopic studies on intact rat renal cortex and medulla, Magn. Reson. Med. 41 (1999) 1108–1118.

[10] S. Garrod, E. Humpher, S.G. Connor, J.C. Connelly, M. Spraul, J.K. Nicholson, E. Holmes, High-resolution ^{1}H NMR and magic angle spinning NMR spectroscopic investigation of the biochemical effects of 2-bromoethanamine in intact renal and heptic tissue, Magn. Reson. Med. 45 (2001) 781–790.
[11] P. Weybright, K. Millis, N. Campbell, D.G. Cory, S. Singer, Gradient, high-resolution, magic angle spinning ^{1}H nuclear magnetic resonance spectroscopy of intact cells, Magn. Reson. Med. 39 (1998) 337–345.
[12] J.L. Taylor, C.L. Wu, D. Cory, R.G. Gonzalez, A. Bielecki, L.L. Cheng, High-resolution magic angle spinning proton NMR analysis of human prostate tissue with slow spinning rates, Magn. Reson. Med. 50 (2003) 627–632.
[13] M.E. Bollard, E.G. Stanley, J.C. Lindon, J.K. Nicholson, E. Holmes, NMR-based metabonomic approaches for evaluating physiological influences on biofluid composition, NMR Biomed. 18 (2005) 143–162.
[14] J.K. Nicholson, I.D. Wilson, High resolution ^{1}H NMR spectroscopy of biological fluids, Prog. NMR Spectrosc. 21 (1989) 449–501.
[15] J.L. Griffin, Metabolic profiles to define the genome: can we hear the phenotypes?, Philos Trans. R. Soc. Lond. B 359 (2004) 857–871.
[16] J.C. Lindon, J.K. Nicholson, E. Holmes, J.R. Everett, Metabonomics: metabolic processes studies by NMR spectroscopy of biofluids, Concepts Magn. Reson. 12 (2000) 289–320.
[17] A. Bax, N.M. Szeverenyi, G.E. Maciel, Correlation of isotropic shifts and chemical shift anisotropies by two-dimensional Fourier-transform magic angle hopping NMR spectroscopy, J. Magn. Reson. 52 (1983) 147–152.
[18] N.M. Szeverenyi, A. Bax, G.E. Maceil, Magic-angle hopping as an alternative to magic angle spinning for solid state NMR, J. Magn. Reson. 61 (1985) 440–447.
[19] C. Keeler, J. Xiong, H. Lock, S. Dec, T. Tao, G.E. Maciel, A new in situ chemical reactor for studying heterogeneous catalysis by NMR: the GRASSHopper, Catalysis Today 49 (1999) 377–383.
[20] J.Z. Hu, A.M. Orendt, D.W. Alderman, C. Ye, R.J. Pugmire, Improvements to the magic angle hopping experiment, Solid State NMR 2 (1993) 235–243.
[21] G.E. Maciel, N.M. Szeverenyi, M. Sardashti, Chemical-shift-anisotropy powder patterns by the two-dimensional angle-flipping approach. Effects of crystallite packing, J. Magn. Reson. 64 (1985) 365–374.
[22] A. Bax, N. Szeverenyi, G.E. Maciel, Chemical shift anisotropy in powdered solids studied by 2D FT NMR with flipping of the spinning axis, J. Magn. Reson. 55 (1983) 494–497.
[23] T. Terao, T. Fujii, T. Onodera, A. Saika, Switching-angle sample-spinning NMR-spectroscopy for obtaining powder-pattern-resolved 2D spectra-measurements of C-13 chemical shift anisotropies in powdered 3,4-dimethoxybenzaldehyde, Chem. Phys. Lett. 107 (1984) 145–148.
[24] T. Nakai, C.A. McDowell, A fast two-dimensional switching-angle sample-spinning method for separating chemical-shift powder patterns, J. Magn. Reson. 93 (1991) 618–623.
[25] A.C. Kolbert, H.J.M. De Groot, R.G. Griffin, Two-dimensional switched-speed spinning NMR, J. Magn. Reson. 85 (1989) 60–68.
[26] R.C. Zeigler, R.A. Wind, G.E. Maciel, The stop-and-go spinning techniques in MAS experiments, J. Magn. Reson. 79 (1988) 299–306.
[27] Z. Gan, High-resolution chemical shift and chemical shift anisotropy correlation in solids using slow magic angle spinning, J. Am. Chem. Soc. 114 (1992) 8307–8309.
[28] Z. Gan, R.R. Ernst, An improved 2D magic-angle-turning pulse sequence for the measurement of chemical-shift anisotropy, J. Magn. Reson. A 123 (1996) 140–143.
[29] Z. Gan, Spinning side-band suppression using a pseudo-2-dimensional experiment, J. Magn. Reson. A 109 (1994) 253–255.
[30] G. McGeorge, D.W. Alderman, D.M. Grant, Resolution enhancement in C-13 and N-15 magic-angle turning experiments with TPPM decoupling, J. Magn. Reson. 137 (1999) 138–143.
[31] J.Z. Hu, W. Wang, F. Liu, M.S. Solum, D.W. Alderman, R.J. Pugmire, D.M. Grant, Magic-angle-turning experiments for measuring chemical-shift-tensor principal values in powdered solids, J. Magn. Reson A 113 (1995) 210–222.
[32] J.Z. Hu, D.W. Alderman, C. Ye, R.J. Pugmire, D.M. Grant, An isotropic chemical shift–chemical shift anisotropy magic-angle slow-spinning 2D NMR experiment, J. Magn. Reson. A 105 (1993) 82–87.
[33] J.Z. Hu, A.M. Orendt, D.W. Alderman, R.J. Pugmire, C. Ye, D.M. Grant, Measurement of ^{13}C chemical shift tensor principal values with a magic-angle turning experiment, Solid State NMR 3 (1994) 181–197.
[34] D.W. Alderman, G. McGeorge, J.Z. Hu, R.J. Pugmire, D.M. Grant, A sensitive, high resolution magic angle turning experiment for measuring chemical shift tensor principal values, Mol. Phys. 95 (1998) 1113–1126.
[35] O.N. Antzutkin, S.C. Shekar, M.H. Levitt, Two-dimensional sideband separation in magic-angle-spinning NMR, J. Magn. Reson. A 115 (1995) 7–19.
[36] A.C. Kolbert, R.G. Griffin, Two-dimensional resolution of isotropic and anisotropic chemical shifts in magic angle spinning NMR, Chem. Phys. Lett. 166 (1990) 87–91.
[37] L. Frydman, G.C. Chingas, Y.K. Lee, P.J. Grandinetti, M.A. Eastman, G.A. Barral, A. Pines, Variable–angle correlation spectroscopy in solid-state nuclear magnetic resonance,, J. Chem. Phys. 97 (1992) 4800–4808.
[38] A.M. Orendt, J.Z. Hu, Y.J. Jiang, J.C. Facelli, W. Wang, R.J. Pugmire, C. Ye, D.M. Grant, Solid-state C-13 NMR measurements in methoxynaphthalenes: determination of the substituent chemical shift effects in the principal values, J. Chem. Phys. A 101 (1997) 9169–9175.
[39] J.C. Facilli, J.Z. Hu, A.M. Orendt, A.M. Arif, R.J. Pugmire, D.M. Grant, Solid-state C-13 NMR, X-ray, and quantum-mechanical studies of the carbon chemical-shift tensors of *p*-tolyl ether, J. Phys. Chem. 98 (1994) 12186–12190.
[40] J.Z. Hu, M.S. Solum, C.M.V. Taylor, R.J. Pugmire, D.M. Grant, Structural determination in carbonaceous solids using advanced solid state NMR techniques, Energy Fuels 15 (2001) 14–22.
[41] J.Z. Hu, D.N. Rommereim, R.A. Wind, High resolution ^{1}H NMR spectroscopy in rat liver using magic angle turning at a 1 Hz spinning rate, Magn. Reson. Med. 47 (2002) 829–836.
[42] R.A. Wind, J.Z. Hu, D.N. Rommereim, High-resolution ^{1}H NMR spectroscopy in a live mouse subjected to 1.5 Hz magic angle spinning, Magn. Reson. Med. 50 (2003) 1113–1119.
[43] J.Z. Hu, R.A. Wind, Sensitivity-enhanced phase corrected ultra-slow magic angle turning using multiple-echo data acquisition, J. Magn. Reson.163 (2003)149–162.
[44] R.A. Wind, J.Z. Hu, P.D. Majors, Slow-MAS NMR: a new technology for in vivo metabolomic studies, Drug Discov. Today Technol. 2 (2005) 291–294.
[45] R.A. Wind, J.Z. Hu, P.D. Majors, Localized in vivo isotropic–anisotropic correlation ^{1}H NMR spectroscopy using ultraslow magic angle spinning, Magn. Reson. Med. 55 (2006) 41–49.
[46] R.A. Wind, J.Z. Hu, *In vivo* and *ex vivo* high-resolution ^{1}H NMR in biological systems using low-speed magic angle spinning, Prog. Nucl. Magn. Reson. Spectrosc. 49 (2006) 207–259.
[47] M. Hunger, T. Horvath, A new MAS NMR probe for *in-situ* investigation of hydrocarbon conversion on solid catalysts under continuous-flow conditions, J. Chem. Soc. Comm. Issue 14 (1995) 1423–1424.
[48] P. Goguen, J.F. Haw, An in situ NMR probe with reagent flow and magic angle spinning, J. Catal. 161 (1996) 870–872.